The Psyche Multispectral Imager Investigation: Characterizing the Geology, Topography, and Multispectral Properties of a Metal-Rich World

J.F. Bell III[1] · M.A. Ravine[2] · M.A. Caplinger[2] · J.A. Schaffner[2] · S.M. Brylow[2] ·
M.J. Clark[2] · D.A. Peckham[2] · P.T. Otjens[2] · G.J. Price[2] · T. Rowell[2] · J.W. Ravine[2] ·
J.D. Laramee[3] · R.C. Juergens[4] · W. Morgan[4] · A.G. Parker[4] · D.A. Williams[1] ·
A. Winhold[1] · S. Dibb[1] · E. Cisneros[1] · M. Walworth[1] · H. Zigo[1] · L. Auchterlonie[1] ·
N. Warner[5] · H. Bates-Tarasewicz[5] · N. Amiri[5] · C. Polanskey[5] · N. Mastrodemos[5] ·
R.S. Park[5] · N.K. Alonge[5] · R. Jaumann[6] · R.P. Binzel[7] · T.J. McCoy[8] · M.G. Martin[5] ·
P.A. Arthur[5]

Abstract

The Psyche Multispectral Imager ("the Imager") is a payload system designed to directly achieve or to indirectly enable the key scientific goals and optical navigation requirements of NASA's Psyche mission, which will conduct the first up-close orbital investigation of the metal-rich Main Belt asteroid (16) Psyche. The Imager consists of a pair of block redundant cameras and electronics that are mounted inside the thermally controlled spacecraft body, with a view out the spacecraft −X panel that will be nadir-pointed during nominal asteroid orbital mapping operations. The two identical Camera Heads are connected to a separate Digital Electronics Assembly (DEA) box that interfaces to the spacecraft avionics and that provides power, commanding, data processing, and onboard image storage. The Imager system shares significant heritage with imaging instruments flown on the *Mars Climate Orbiter*, the *Mars Science Laboratory* and *Mars 2020* rovers, and *Juno*. Each camera consists of a 1600×1200 photosensitive pixel charge-coupled device (CCD) detector and its associated electronics, a 9-position filter wheel assembly, a compact catadioptric $f/2.9$ telescope with a fixed focal length of 148 mm, and a sunshade to minimize stray and scattered light. The Imager CCD, filters, and optics enable broadband polychromatic ($\sim540 \pm 250$ nm) imaging plus narrowband imaging in 7 colors centered from 439 to 1015 nm. An additional neutral density filter enables protection of the CCD from direct solar illumination. Each camera has a field of view of $4.6° \times 3.4°$ and an instantaneous field of view of 50 μrad/pixel that enables imaging of the asteroid at scales ranging from ~35 m/pix from 700 km altitude to ~4 m/pix at 75 km altitude. The primary camera ("Imager A") is pointed along the spacecraft −X axis, and the backup camera ("Imager B") is toed-out by 3.7° to potentially enable greater surface area coverage per unit time if both Imagers are operated simultaneously during some mission phases. Stereoscopic mapping is performed by observing the same surface regions with either camera over a range of off-nadir pointing angles.

Keywords Asteroids · (16) Psyche · Psyche mission · Space instrumentation · Space imaging

Extended author information available on the last page of the article

Springer

1 Introduction

The NASA Psyche Discovery mission (Elkins-Tanton et al. 2020; Polanskey et al. 2025) will conduct the first detailed, *in situ* exploration of an asteroid interpreted to have a composition significantly dominated by metal. Asteroid (16) Psyche, the largest of the M-class asteroids (∼225 km diameter), is thought to either be the exposed core of a pre-existing larger differentiated body or composed of primordial material having accreted from highly reduced metal-rich nebular condensates (e.g., Elkins-Tanton et al. 2020, 2022). The Psyche orbital mission was selected for flight in 2017 as the 14th of the NASA Discovery series of competed, principal investigator-led missions. The spacecraft launched in October 2023 and, after a Mars flyby gravity assist in 2026, will arrive at Psyche (in the Main Belt at ∼3 AU heliocentric distance) in mid 2029.

A key payload element required for addressing the science goals and objectives of the Psyche mission is a visible to short-wavelength near-infrared multispectral imaging system known as the Psyche Multispectral Imager (or just "the Imager" for short). The Imager will acquire data needed to characterize the shape, topography, geology, and (to a limited extent) surface compositional variations of Psyche. Here, we describe the specific science goals, measurement requirements, design, testing, and planned capabilities of the Imager, as well as the kinds of science products it will generate and the kinds of results that it is expected to obtain.

2 Psyche Multispectral Imager Science Goals and Objectives

2.1 Psyche Mission Science Goals and Objectives Related to Imaging

Table 1 summarizes the high-level science goals of the Psyche mission, as well as the specific more detailed Psyche mission science objectives that drove the choices of payloads and measurements needed to reach these goals (e.g., Polanskey et al. 2025). In addition, the specific goals of the Psyche Multispectral Imager investigation are also listed in Table 1, and described in more detail below. As also described in detail below, the Psyche Multispectral Imager investigation provides critical data to address all three of the mission's primary science goals as well as four of its five driving objectives (Objectives A, B, D, and E in Table 1).

2.2 Imager Scientific Investigation Objectives

2.2.1 Geology/Geomorphology

A primary Psyche Multispectral Imager science objective is to characterize the geology and geomorphology of a never-before-seen kind of object: a metallic world (e.g., Marchi et al. 2022; Jaumann et al. 2022). Is the geology of Psyche similar to that of a stony or icy small body, or is its surface geomorphology radically different from that of other known worlds? How do craters, structural features, and/or erosional landforms scale to a body with potentially significantly different physical and compositional properties? Is there geologic evidence for events (e.g., cratering, brecciation, faulting) that could have disrupted or modified any potential magnetization? The Imager investigation will directly address these kinds of questions by acquiring broadband visible-wavelength, multi-look angle images that will enable mapping at the required few to tens of meters/pixel spatial scales and derivation of

Table 1 *Psyche* Mission and Imager Investigation Science Goals and Objectives

Psyche Mission Science Goals

Goal 1	Understand an unexplored building block of planet formation: Iron cores
Goal 2	Look inside the terrestrial planets, including Earth, by directly examining the interior of a differentiated body, which otherwise could not be seen
Goal 3	Explore a new type of world for the first time by examining a small body made not of rock or ice, but one that is metal-rich

Psyche Mission Science Objectives

Objective A	Is Psyche the core of a differentiated planetesimal?
Objective B	What are the relative ages of surface regions on the asteroid?
Objective C	What are the abundances of light elements on the asteroid's surface?
Objective D	Did Psyche form in oxidizing or reducing conditions?
Objective E	What is the nature of Psyche's detailed surface geomorphology and topography?

Psyche Multispectral Imager Investigation Objectives

(1)	Characterize the geology and geomorphology of (16) Psyche
(2)	Derive the surface topography and shape of (16) Psyche
(3)	Search for and characterize the nature of metal-silicate mixing on (16) Psyche's surface
(4)	Search for and detect any diagnostic sulfide minerals on (16) Psyche's surface
(5)	Acquire images to support optical navigation and orbital spacecraft operations

$\leq$50 m required vertical precision Digital Terrain Models (DTMs). The Imager's pixel scale and DTM requirements are based on experience from previous imaging investigations of planetary and especially small body surfaces, and are intended to enable the detailed analysis of impact cratering and any volcanic, tectonic, and/or gradational processes on this unique world at the appropriate scales (e.g., Sullivan et al. 2002; Marchi et al. 2022, 2023; Jaumann et al. 2022).

Another major mission objective relevant to imaging is characterization of the relative ages of Psyche's surface regions (Marchi et al. 2022). The Imager will contribute to this mission objective by mapping $\geq$50% of the asteroid's surface in the broadband filter at a scale of $\leq$200 m/pix (Polanskey et al. 2025), enabling the counting and characterization of craters with diameters larger than 1 km. This range of crater sizes will also enable assessment of the potential crustal implications of the simple to complex crater transition for an object of this size, as well as the assessment of materials potentially excavated from depth (e.g., Bottke et al. 2020; Marchi et al. 2022). Imager data will also be used to construct a global geologic map of the surface (Polanskey et al. 2025), and potentially to define a global chronostratigraphy as was done, for example, by the Dawn mission at the asteroid Vesta (cf., Williams et al. 2014).

2.2.2 Topography and Shape

The Imager's observations of Psyche will also be designed to enable the derivation of the asteroid's surface topography and shape, using a combination of stereo photogrammetry (SPG; geometrical analysis of the parallax of surface features observed over a range of stereo convergence angles; see e.g., the review in Jaumann et al. 2022), and stereo photoclinometry (SPC; "shape from shading", or the analysis of brightness variations of surface features

observed over a range of solar illumination conditions; e.g., reviews in Zuber et al. 2022 and Jaumann et al. 2022).

The Imager's combination of high-resolution (≤20 m/pix) broadband images, mosaics of the landforms, and topographic maps of the surface of Psyche (from digital terrain models with height accuracy of 50 m or smaller), will enable lower spatial resolution gravity field (Zuber et al. 2022) and neutron/gamma-ray compositional measurements (Lawrence et al. 2025) to be correlated with surface geology, providing further insights into the asteroid's internal structure and homogeneity.

2.2.3 Mineralogy and Composition

Because of the inferred relatively high metal abundance of Psyche (based on its visible to near-IR reflectance spectrum, relatively high density, and high radar reflectivity; e.g., Elkins-Tanton et al. 2020), a major goal of the Psyche mission is to test the hypotheses that the asteroid is or is part of a differentiated planetesimal core, or that it is not a core but is instead a different class of object composed of a significant fraction of primordial unmelted metal (e.g., Elkins-Tanton et al. 2022). The Imager's observations can address these hypotheses by using multispectral imaging to search for and characterize the nature of any large-scale metal-silicate mixing on the asteroid's surface.

Specifically, visible to near-infrared multispectral imaging at key wavelengths between 450 to 1000 nm (Table 2; Fig. 1) can enable the detection of re-accreted, exogenically-supplied, or impact-exposed iron-bearing silicate minerals like pyroxene and (to a lesser extent) olivine, and mapping of the asteroid's spectral properties in this wavelength range can quantify the degree of mixing of these kinds of silicates with metals on the surface (e.g., Cloutis and Gaffey 1991; Cloutis et al. 2010; Dibb et al. 2022, 2023). The Imager will observe the surface at key wavelengths and at a spatial resolution ≤ 500 m/pix. Modeling of the expected Imager performance [assuming Signal to Noise Ratio (SNR) ≥ 50 in all filters] indicates that even relatively weak absorption features seen in laboratory and meteorite metal + silicate mixture spectra with iron-bearing silicate abundances of only ≈5–10 wt.% (depending on specific compositions and silicate grain sizes) will be detectable in the Imager's spectroscopic band ratios and band depth maps (e.g., Dibb et al. 2023).

In addition to silicate detection and mapping, the Imager will also address the Psyche mission objective of determining whether Psyche was formed under conditions more oxidizing or more reducing than Earth's core by searching for and detecting diagnostic sulfide minerals like troilite (FeS) and oldhamite [(Ca,Mg,Fe)S] (e.g., Dibb et al. 2021). The presence of such cubic monosulfide phases has been interpreted to be consistent with highly reducing formation conditions (e.g., Clark et al. 2004; Fornasier et al. 2008, 2010; Elkins-Tanton et al. 2020; McCoy et al. 2022). To search for sulfides, the Imager will use narrow-band filters to detect and map a weak cubic monosulfide feature that has been identified in laboratory and telescopic data in the 435-550 nm wavelength region (e.g., Gaffey et al. 1993; Burbine et al. 2002; Clark et al. 2004). Spectroscopic ratio and band depth analyses of these images are expected to enable the search for signatures of S-bearing phases on Psyche with local mixture abundances ≳ 10 wt.% (Elkins-Tanton et al. 2022; Dibb et al. 2023).

2.3 Imager Optical Navigation and Orbital Operations Support Objectives

The Imager also serves as the primary Optical Navigation ("OpNav") camera system for the Psyche mission. OpNav is an essential component of mission design and navigation and will be used during the Approach phase and all Science orbits (see Sect. 5 below). OpNav

Table 2 Psyche Multispectral Imager Filter Bandpass Data

Filter #	Imager A (primary)			Imager B (backup)			Justification (see text for details)
	Band Center[1]	Effective Center at Psyche[2]	FWHM[3]	Band Center[1]	Effective Center at Psyche[2]	FWHM[3]	
	(nm)	(nm)	(nm)	(nm)	(nm)	(nm)	
0	–	–	–	–	–	–	Neutral Density 5 (factor of 10^{-5}) Sun blocking filter
1	539	540	259	538	539	250	Broadband polychromatic bandpass for maximum sensitivity OpNav, topography, and geologic imaging
2	439	442	49	439	441	48	Sulfide detection
3	494	494	24	493	493	24	Sulfide detection
4	548	548	24	548	548	24	Sulfide detection
5	722	722	40	723	722	40	Reflectance continuum for 1000 nm features
6	841	840	48	842	841	48	Detection of Fe-bearing silicates
7	942	942	46	942	941	46	Detection of Fe-bearing silicates
8	1015	1014	40[4]	1015	1014	41[4]	Detection of Fe-bearing silicates

[1]Band Center calculated as the wavelength corresponding to 50% of the integral under the full system's filter profile, which is the measured system-level bandpass that includes the filter, optics transmission, and CCD quantum efficiency.

[2]Effective centers are computed after convolution of each full system filter profile with the solar spectrum and assuming a linearly increasing albedo of (16) Psyche of 0.11–0.15 between 442–1014 nm, based on the summary by Dibb et al. (2023).

[3]Full Width at Half Maximum, calculated using the same effective bandpass approach outlined in Note 2.

[4]Filter 8 is significantly asymmetric on its longer wavelength side, and so the traditional concept of FWHM does not accurately capture its full range of responsivity. See Winhold et al. (2025) for additional details.

data are used in conjunction with radio tracking data in the orbit determination process. The key OpNav functions during Psyche operations are: (1) Continuously supporting real-time orbit determination to assist in updating the science instrument sequences, pointing and data acquisition, in-orbit trajectory correction maneuvers, successful entry into initial orbit, and transfers between science orbits; (2) Assisting in the science orbit reconstruction at the end of each orbit phase; and (3) Characterizing key physical properties of Psyche, such as the spin state and the global shape of the asteroid that are used by both the mission design and science planning teams.

In addition, during the Cruise phase of the mission, OpNav will support imaging of stars and star clusters and data analyses that can be used to assess spacecraft pointing accuracy and jitter, radiometric responsivity and stability, and the nature of any geometric distortion across the Imager field of view (Winhold et al. 2025). The accuracy of the geometric camera models is of particular importance to OpNav to enable high-quality astrometric optical data analysis. Specifically, the goal for the camera geometric model is to be of sufficient accuracy so as not to limit the expected astrometric accuracy of Imager observations in the clear filter,
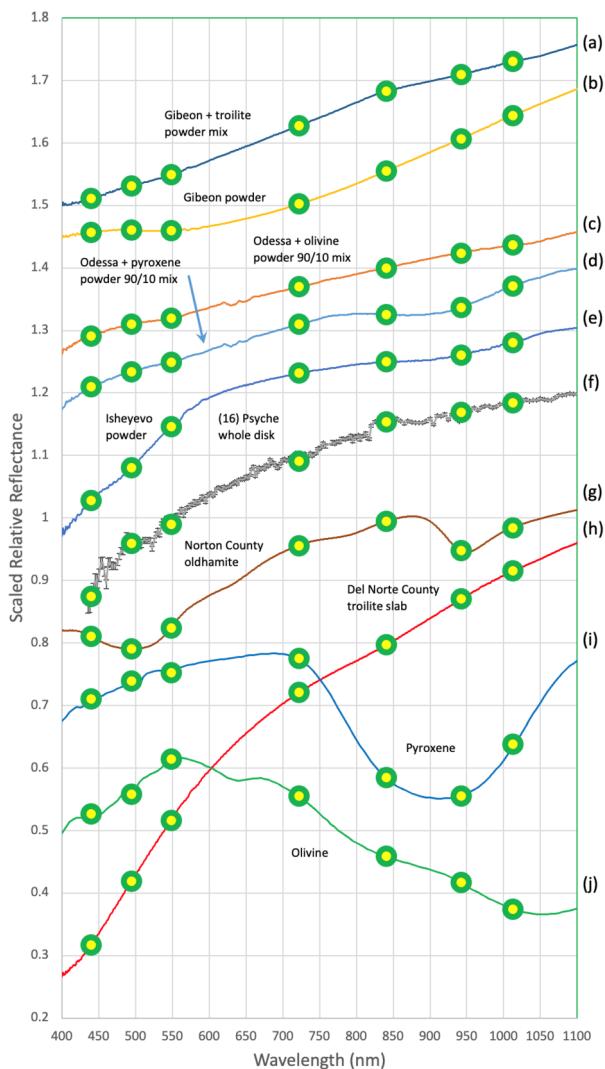
Fig. 1 Examples of relevant high resolution visible to near-IR telescopic, meteorite, and laboratory mineral or mineral mixture spectra (solid lines) resampled over the bandpasses of the Psyche Multispectral Imager's narrowband filters (green/yellow data points; Table 2). These examples include many of the "best matches" to the telescopic spectrum of (16) Psyche compiled in Table 3 of Dibb et al. (2023). All spectra have been scaled to 1.0 at 550 nm and then vertically offset for clarity. Spectra and sources: (a) 80/20 wt.% mixture of < 75 μm grain size powders of the metallic meteorite Gibeon and troilite, from Dibb et al. (2021); (b) Powdered > 75 μm grain size sample of Gibeon, from Dibb et al. (2023): (c) 90/10 wt.% mixture of < 45 μm grain size powders of the metallic meteorite Odessa and olivine, from Cloutis et al. (2009); (d) 90/10 wt.% mixture of < 45 μm grain size powders of the metallic meteorite Odessa and low-Fe pyroxene, from Cloutis et al. (2009); (e) Powdered > 75 μm grain size sample of the CH/CBb chondrite Isheyevo, from Dibb et al. (2023); (f) whole-disk telescopic spectrum of (16) Psyche from the SMASSII survey of Bus and Binzel (2002); (g) Powdered < 1 mm oldhamite-dominated clasts from the Norton County aubrite, from by Dibb et al. (2022); (h) 1200 grit polished troilite slab, from Dibb et al. (2023); (i) Low-Fe < 45 μm pyroxene powder (PYX042) used in mixture (d), from Cloutis (2002): (j) Olivine < 45 umpowder (OLV003) used in mixture (c), from Cloutis et al. (2009)

which from systematic navigation studies from prior small body orbital missions has been shown to be in the range of 0.2-0.1 pixels, in the various stages of orbital operations (e.g., Mastrodemos et al. 2012, 2015).

During the initial approach to the asteroid, the optical data will consist of the estimated center of the body based on limb-fitting and image cross-correlation methods, using an *a priori* shape model. After Psyche exceeds ∼50 pixels in diameter and through to the end of the mission the optical data will include specifically defined landmarks, constructed from DTMs of the surface using the SPC methodology (e.g., Sect. 2.2.2; Jaumann et al. 2022; Zuber et al. 2022). These DTMs will be synthesized into global shape models. Similar landmark-based navigation was carried out with the *Dawn* mission (e.g., Mastrodemos et al. 2012) and to first order the overall process for the Psyche mission will be similar.

2.4 Imager-Specific Design Considerations and Requirements

To help accomplish the scientific goals and objectives of the Psyche mission and the Imager investigation listed in Table 1, the cameras must be able to observe the surface of Psyche from orbit in an approximately nadir-pointed attitude, through a broadband ("clear") filter that enables maximum light collection over minimum exposure times, and through a variety of narrowband color filters optimized to detect specific kinds of diagnostic silicate and sulfide minerals. In addition, the Psyche spacecraft must enable the Imagers to observe the same regions of the surface at multiple off-nadir angles to enable the creation of DTMs using image-based SPG or SPC methods. Stereo imaging will nominally be performed by using just one camera and operationally acquiring ≥4 images of each surface element at nadir and at up to ±20° stereo separation. And as noted above, the Imagers will also be needed for OpNav during cruise, and to provide geologic context for measurements made by the other Psyche mission science investigations.

A detailed set of multi-level Psyche mission and measurement requirements was established and linked to the mission's specific scientific goals and objectives (Table 1) with appropriate margins to guide the design, testing, and eventual operation of all the science instruments on the Psyche spacecraft (e.g., Polanskey et al. 2025). The specific Project requirements levied on the Imager investigation are outlined in Table 3. Imager-specific requirements span the range from contributions to high-level mission-critical science (Level 1 requirements), to measurement requirements needed to meet specific Imager-related mission science objectives (Level 2), to requirements placed on other subsystems within the mission that help enable the Imager to meet specific mission science objectives (Level 3), and finally to detailed requirements on specific individual Imager components, subsystems, or tests that ensure that the as-built Imagers achieve the required level of performance and accuracy to meet Imager investigation goals (Level 4).

3 Instrument Description and Heritage

3.1 Overview

The Psyche Multispectral Imager subsystem is a compact, low mass, and power efficient pair of block-redundant Charge-Coupled Device (CCD) imaging cameras, filter wheels, and electronics that provide a low risk, high heritage way to meet the Psyche mission's imaging-related requirements (Table 3). While the Imagers are not exact copies of any previously-flown instruments, heritage for their CCD sensors, electronics, filters, filter wheel mechanisms, and flight software comes primarily from the *Mars Science Laboratory* (*MSL*) mission's Mastcam, MAHLI, and MARDI imaging systems (Malin et al. 2017) and the *Mars*

Table 3 Psyche Mission and Instrument Requirements Relevant to the Psyche Multispectral Imager

| Level[a]	Requirement	Notes and Traceability to Mission Objectives[b]
1	Determine whether there are contiguous silicate regions on scales larger than 1 km, where silicates are defined as having >14% Si by mole.	*Objective A*: Metal/silicate mixing. Multispectral filters used to search for and map regions containing iron-bearing silicate minerals like pyroxene and olivine.
1	Determine the relative ages of regions of the surface of Psyche by counting craters with diameters larger than 1 km over at least 50% of the surface.	*Objective B*: Relative ages. Clear filter used to map the surface between ≈35 m/pix (Orbit A) to ≈3.5 m/pix (Orbit D), to identify geologic features such as craters.
1	Determine whether Psyche has >10 ± 5 wt.% sulfides like oldhamite (global average), indicating highly reducing conditions.	*Objective D*: Oxidizing vs. reducing conditions. Multispectral filters used to search for and map regions containing sulfides.
1	Characterize Psyche's topography over 50% of the surface at ≤200 m/pix horizontal and ≤50 m vertical resolution.	*Objective E*: Surface topography. Influences optics and orbital altitude (pixel scale), off-nadir pointing capability of the spacecraft (multiple look angles to produce DTMs using stereo photogrammetry and stereo photoclinometry), and system responsivity (clear filter, sensor, and electronics).
2	The Psyche Project shall map the metal to silicate fraction of at least 80% of (16) Psyche's surface (with filters near 725, 850, 948 and 1041 nm) at a pixel scale ≤ 500 m and SNR ≥ 50.	*Objective A*: Metal to silicate mixing. Influences optics and orbital altitude (pixel scale), system responsivity, and need for specific near-IR filters.
2	The Psyche Project shall map ≥80% of (16) Psyche's surface with the clear filter at a pixel scale of ≤20 m and SNR ≥ 50.	*Objective E*: Surface geology. Influences optics and orbital altitude (pixel scale), and system responsivity.
2	The Psyche Project shall determine the shape of (16) Psyche by mapping with the clear filter over at least 80% of its surface with a pixel scale ≤ 200 m/pix and SNR ≥ 50 to obtain ≤70 m vertical accuracy using stereo imaging techniques.	*Objective A*: Determine density (mass/volume). Influences optics and orbital altitude (pixel scale), off-nadir pointing capability of the spacecraft, and system responsivity.
2	The Psyche Project shall map (16) Psyche's surface features with the clear filter over ≥50% of its surface with a pixel scale ≤ 20 m/pix and SNR ≥ 50 to obtain ≤50 m vertical accuracy using stereo imaging techniques.	*Objective E*: Surface topography. Influences optics and orbital altitude (pixel scale), off-nadir pointing capability of the spacecraft, and system responsivity.
2	The Psyche Project shall map at least 50% of (16) Psyche's surface with the clear filter at a pixel scale ≤ 200 m/pix and SNR ≥ 50 to support crater age determination.	*Objective B*: Relative ages. Influences optics and orbital altitude (pixel scale) and system responsivity.
2	The Psyche Project shall map at least 80% of (16) Psyche's surface (with filters near 437, 495, and 550 nm) at a pixel scale ≤ 200 m/pix and SNR ≥ 50 to search for evidence of oldhamite.	*Objective D*: Oxidizing vs. reducing conditions. Influences multispectral filters used to search for and map sulfides, optics and orbital altitude (pixel scale), and system responsivity
3	The Spacecraft shall accommodate operating Imager A and Imager B simultaneously.	*Objective E*: Geology and topography. Simultaneous operation of both Imagers allows more clear filter mapping per unit time in Orbit D, closest to the asteroid.

Table 3 (*Continued*)

Level[a]	Requirement	Notes and Traceability to Mission Objectives[b]
3	Imager A boresight and Imager B boresight are "toed out" relative to each other such that Imager A is mounted nominally nadir (boresight parallel to the spacecraft −X axis) and Imager B is mounted with a toe-out angle of $3.7° \pm 0.4°$.	*Objective E*: Geology and topography. Toe-out and simultaneous operation of both Imagers enables $\approx 1.9\times$ surface area coverage per unit time in Orbit D.
4	The images shall have an average signal to noise ratio of greater than or equal to 50:1 in each spectral band.	*Objectives A and D*: Metal/silicate mixing and sulfides. Influences system responsivity (filter bandwidths, sensor, and electronics).
4	Each Imager instrument Instantaneous Field of View (IFOV) shall be smaller than or equal to 50 µrad $\pm 2\%$.	*Objectives A, B, D, E*: Metal/silicate mixing, relative ages, sulfides, geology/topography: Spatial resolution requirements drive optics design.
4	Each Imager shall provide a Field of View (FOV) of $4.4° \times 3.3° \pm 2\%$.	*Objectives A, B, D, E*: Metal/silicate mixing, relative ages, sulfides, geology/topography: Surface coverage requirements drive optics design
4	Each Imager shall have a Modulation Transfer Function (MTF) performance of >0.2 at Nyquist (67.6 lp/mm) over a required scientific operating range of $-10\,°C$ to $+25\,°C$	*Objectives A, B, D, E*: Metal/silicate mixing, relative ages, sulfides, geology/topography: Spatial resolution requirements drive optics design.
4	The Imager data shall be radiometrically accurate to $\leq 10\%$ absolute and $\leq 2\%$ relative radiance (pixel to pixel and band to band) through each spectral band across the full FOV.	*Objectives A and D*: Metal/silicate mixing and sulfides. Influences system responsivity (filter bandwidths, sensor, and electronics).
4	Distant imaging of representative natural scenes and/or color/reflectance standards shall be used to validate the radiometric calibration of the Imager.	*Objectives A, D, and E*: Metal/silicate mixing, sulfides, topography from stereo photogrammetry. Influences system responsivity (filter bandwidths, sensor, and electronics).

[a]See text for details; [b]See Table 1.

2020 mission's Mastcam-Z imaging system (Bell et al. 2020), which were also built by Malin Space Science Systems, Inc. (MSSS), with only slight changes in filter wavelengths needed to meet Psyche-specific multispectral imaging requirements. Indeed, the Imager uses exactly the same high-heritage interface to the Psyche spacecraft avionics as the *MSL* and *Mars 2020* heritage cameras used with those NASA Jet Propulsion Laboratory (JPL) rover spacecraft; this was part of the justification for selecting this system as part of a spacecraft also to be operated with JPL avionics. Additionally, partial heritage for the Imager optics comes from the *Mars Climate Orbiter* mission's Mars Color Imager medium angle imaging system (Malin et al. 2001), also a previously built MSSS instrument, but with a slightly different lens prescription for the Imager to meet Psyche-specific spatial resolution requirements.

The Imager system consists of four components: Two identical 148-mm focal length $f/2.9$ Camera Heads, each consisting of a camera electronics box with a 1648×1214 total pixel (1600×1200 unmasked, photoactive pixels) focal plane array CCD, a filter wheel assembly including 9 rectangular glass-coated interference filters driven by a CDA Inter-Corp GZ4 16:1 gear ratio stepper motor actuator, an optics/Sun shade assembly, and an electronics card housing motor drivers, flash memory, and SDRAM controlled by a Xilinx Virtex-2 Field Programmable Gate Array (FPGA). The purpose of the second Camera Head is to provide redundancy primarily for mission-critical OpNav, as was done on the *Dawn*
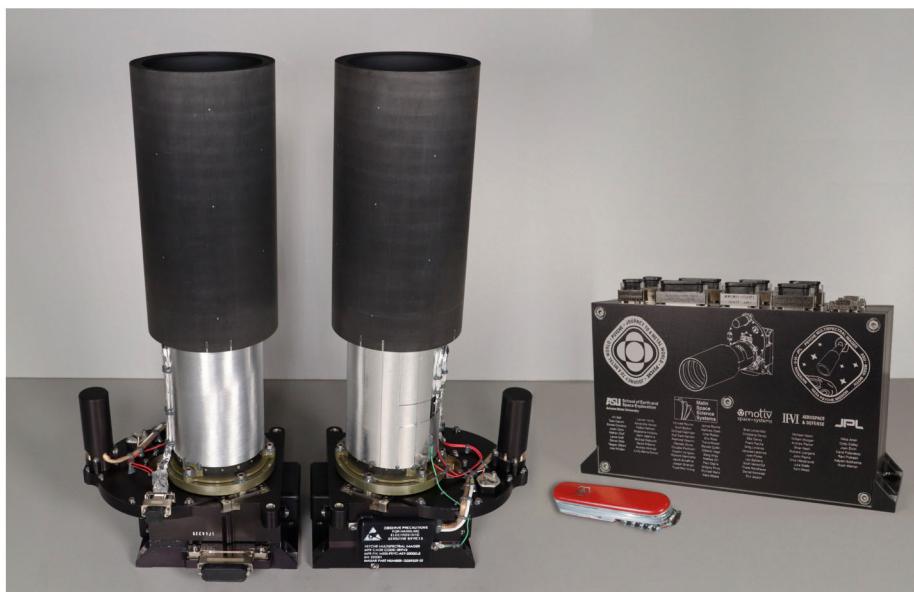
Fig. 2 Flight Psyche Multispectral Imager Camera Heads (left) and flight Digital Electronics Assembly (right), prior to integration with the spacecraft. For scale, the pocket knife is 3.5 inches (90 mm) long

mission; redundancy for science is a secondary benefit. The two independent Imager electronics cards are housed in a single separate Digital Electronics Assembly (DEA) box. The onboard DEA hardware and software enables lossless predictive or lossy JPEG compression, a limited amount of image processing (e.g., subframing, multi-pixel summing, as well as "companding" – a term for compressing to a smaller bit depth then later expanding back to the original bit depth; e.g., Bell et al. 2017), and storage/manipulation of ∼4000 full-frame uncompressed 12-bit images in each camera's flash memory prior to transfer to the spacecraft for downlink. The two flight Imager Camera Heads and the flight DEA are shown in Fig. 2.

3.2 Imager Electronics

As shown in Fig. 3, the Imager electronics are partitioned into two subsystems: the Camera Head (CH) electronics and the Digital Electronics Assembly (DEA). As noted above, both subsystems are very similar to those used previously for cameras on the *MSL* and *Mars 2020* missions, but both subsystems were modified slightly to address issues with parts obsolescence and to improve reliability. Most of the changes involved power circuits: different voltage regulators and passive filters in the CH and a different DC-DC converter architecture in the DEA. Also, the earlier instruments had internal power switching to allow the DEA to operate with the CH turned off, for power management purposes specific to rover operations constraints. Such constraints were not relevant for Psyche mission operations, and thus the internal power switching was removed for the Imager implementation, meaning that both electronics subsystems are powered on when the spacecraft's Imager power switch is enabled. The robustness of the electronics to radiation during the long Psyche mission cruise and operations phases has been demonstrated by the successful performance of the identical electronics used for the *Juno* mission's JunoCam instrument investigation during cruise
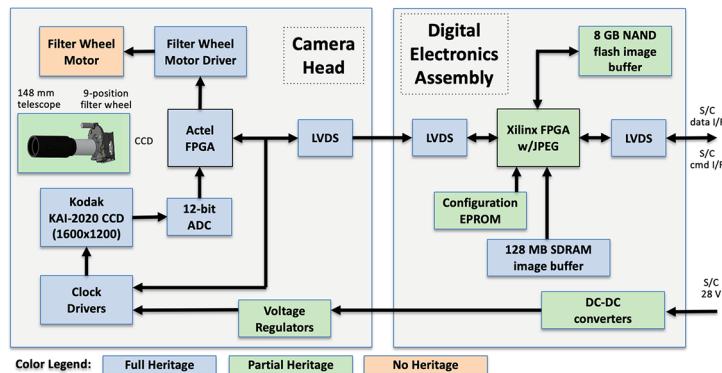
Fig. 3 Block diagram for the two fully redundant Psyche Multispectral Imager Camera Heads and their associated Digital Electronics Assembly (DEA) electronics

and at Jupiter (e.g., Hansen et al. 2017). Specifically, during more than 6 years of Primary and Extended Mission operations in the extremely harsh radiation environment of Jupiter, JunoCam experienced an estimated cumulative dose of ∼28 KRad(Si) behind 1.5 inches of Aluminum shielding before experiencing its first radiation-induced anomaly (Schaffner et al. 2025). In contrast, the mission expected shielded dose for the Imager electronics is estimated to not exceed only ∼3.5 KRad(Si), partly because the electronics are housed relatively deep inside the body of the spacecraft itself (see Sect. 3.6).

3.2.1 Camera Head (CH) Electronics

The CH electronics are designed around the ON Semiconductor (formerly Kodak) KAI-2020M CCD image sensor. This sensor has 1648×1214 pixels (1600×1200 photoactive), each with a 7.4-μm pitch, and uses interline transfer in single output mode to implement electronic shuttering. Unlike its heritage predecessors on *MSL* and *Mars 2020*, which used the Bayer-pattern color variant, this sensor is monochrome. The sensor has microlenses to improve its quantum efficiency, which has a peak of about 55% at around 500 nm (see Fig. 10 in ON Semiconductor Inc 2015). The "fast-dump" capability of the sensor is used to clear residual charge prior to integration and also allows vertical sub-framing of the output image, if commanded.

The output signal from the CCD is AC-coupled and then amplified. The amplified signal is digitized in an Analog to Digital Converter (ADC) circuit to 12 bits at a maximum rate of 10 Mpix/sec. For each pixel, both reset and video levels are digitized and then subtracted in the digital domain to perform correlated double sampling (CDS) that nominally yields an output signal encompassing the full dynamic range between black and full well within 11 bits, from 0-2047 Data Numbers (DN). The CH readout rate can be selected from values of 2.5, 5, and 10 Mpix/sec. For the Psyche mission, the 5 Mpix/sec rate is used by default, as pre-flight characterization testing showed that this provides the best noise performance. Based on performance of this sensor on previous missions, our expectation for initial exposure time modeling was that it would deliver a gain of ∼16 e$^-$/pix, read noise ≤15 e$^-$, and full well ∼30,000 e$^-$. As described in Sect. 4.2, all of these expectations have been met during actual pre-flight and in-flight performance.

All CH functions are supervised by a single Actel RTSX FPGA. In response to commands from the DEA, the FPGA generates the CCD clocks, reads samples from the ADC

and performs digital CDS, and transmits the pixels to the DEA. The FPGA is also responsible for operating the stepper motor for the filter wheel mechanism.

The CH operates using regulated 5 V and ± 15 V power provided by the DEA. A platinum resistance thermometer (PRT) mounted next to the CCD on the camera focal plane is read by the spacecraft to provide temperature knowledge for radiometric calibration. An additional pair of PRTs and redundant etched-foil heaters are attached to the outside of each Camera Head and are thermostatically controlled by the spacecraft to remove moisture from the metering structure of the optics during a bakeout procedure that was conducted shortly after launch.

The CH electronics are laid out as a single rigid-flex printed circuit board (PCB) with three rigid sections. The sections are sandwiched between housing partitions that provide mechanical support and radiation shielding, and the flexible interconnects are enclosed in metal covers (Fig. 4). Each Imager CH assembly bolts to the spacecraft via four feet on its base housing.

3.2.2 Digital Electronics Assembly (DEA) Electronics

The DEA interfaces the Camera Heads to the spacecraft avionics. Each redundant interface from the Imager to the Psyche spacecraft is two (one each for command and telemetry) four-signal flow-controlled LVDS synchronous-serial links, running at 8.25 Mbit/s maximum.

The data interface between the DEA and each CH is a three-signal LVDS synchronous serial link transmitting commands from the DEA to the CH at 2 Mbit/sec and an 8-signal synchronous 6-bit parallel interface from the CH to the DEA at selectable rates from 30 to 120 Mbit/sec (5 to 20 MHz). The DEA is powered from the spacecraft 28 V power bus, provides regulated power to the CHs, and contains a PRT for temperature monitoring.

The core functionality of the DEA is implemented in a Xilinx Virtex-II FPGA. All interface, compression, and timing functions are implemented as logic peripherals of a Microblaze soft-processor core in the FPGA. The DEA provides an image-processing pipeline which includes 12-to-8-bit companding of input pixels based on pre-defined onboard lookup tables; horizontal sub-framing; 2×2, 3×3, or 4×4 pixel summing; and optional lossless predictive or lossy JPEG compression. The image-processing pipeline can run at the full speed of the CH input, writing the processed data stream directly into the DEA memory.

The DEA memory subsystem contains 256 MB of DRAM and 8 GB of non-volatile NAND flash memory. The flash is organized as a large image buffer, allowing images to be acquired without the use of spacecraft memory resources at the maximum camera data rate. The DRAM is typically used as scratchpad space and to store file system information, but can also be used as a buffer for a small number of images, if needed.

The DEA electronics for each Imager are laid out on a single rectangular PCB. The DEA boards for both Imagers are integrated into one unit to save mass. Each PCB is sandwiched between housing sections, and the entire assembly bolts onto a mounting plate inside the $+Y$ panel of the spacecraft (Fig. 5).

3.3 Flight Software

DEA hardware functions are coordinated by the DEA flight software (FSW), which runs on the Microblaze. The FSW receives and executes commands from the spacecraft and transmits any resulting data. The FSW can also implement autoexposure algorithms for image acquisition, perform error correction on the contents of the flash, and implement mechanism control and fault protection. The FSW consists of about 10,000 lines of ANSI C code. Nearly

all the code was inherited without modification from the earlier heritage instruments. New developments included additional fault protection, control of the nine-position filter wheel and motor (the heritage filter wheels had eight positions), addition of 3×3 summing capability, and removal of color processing and other mission-specific functions not needed for Psyche (such as focus and zoom control and focus stack merging).

The Imager FSW also allows considerable flexibility for image acquisition. Images can be acquired in uncompressed form, stored in the DEA flash buffer, and transmitted to the spacecraft multiple times using different compression factors or summing modes. Alternatively, images can be compressed during acquisition and stored as JPEGs in the DEA flash to minimize the amount of buffer space they occupy; the latter capability is useful for video sequences, for example.

3.4 Filter Wheel Mechanism

Each Imager Camera Head includes a nine-position filter wheel (Table 2 and Fig. 4), controlled using a CDA Model GZ4 0.5-inch diameter three-phase stepper motor. The motor drives an integral gear on the outer diameter of the filter wheel, and the wheel itself is supported by a bearing on its inner diameter. Position sensing of the wheel is done using a Hall-effect sensor and magnet pairs at each filter location, with an extra magnet pair for absolute indexing. This mechanism is similar to and based on the ones used for the earlier Mastcam and Mastcam-Z instruments, but using a new motor (because the heritage motors could not be delivered on our required schedule), an additional filter (an opaque Sun-blocking filter to accommodate the need to occasionally "Sun-safe" the optics, a requirement imposed by the spacecraft's solar-electric propulsion system), and a new mounting accommodation for the Imager's specific optics. A flight qualified CDA motor with the same specifications as the flight motors was taken through a life testing program in November 2019. No anomalies were observed during $3 \times$ nominal required lifetime testing of the motor and filter wheel mechanisms.

3.5 Imager Optics and Optomechanical Design

The Imager optics (Fig. 4) consists of a catadioptric telescope with spherical fused silica optical elements providing a fixed focal length of 148 mm, an f/# of 2.9, and a T/# [defined as $(f/\#) \times$ (system transmission)$^{-0.5}$] of 4.7 based on the combination of optics transmittance and the telescope's large central obscuration. The optics yield an Instantaneous Field of View (IFOV) or ground sampling distance of 50 μrad/pix (yielding 3.5 m/pix sampling from an altitude of 70 km), a field of view (FOV) of $4.6° \times 3.4°$, and a depth of field from ∼800 m to infinity. The telescope's focus is fixed and set by the use of a precision-machined focus spacer/light shield located just above the image sensor.

In order to be able to achieve excellent image contrast in family with numerous previous deep space imaging systems, the optics are required to deliver a Modulation Transfer Function (MTF) performance > 0.2 at the Nyquist frequency of the sensor (67.6 lp/mm) and over the required operating range for scientific observations of -10 °C to $+25$ °C. The corresponding Point Spread Function (PSF) requirement was set as a FWHM of < 3 pixels, to provide a good combination between the accuracy of astrometric center finding for OpNav on approach to (16) Psyche and adequate topographic resolution of an extended body during proximity operations (e.g. Mastrodemos et al. 2012, 2015). As described in Winhold et al. (2025), both flight Imagers exhibit PSFs with FWHM ∼2 pixels based on both pre-flight testing using point source targets and in-flight testing using imaging of stars.
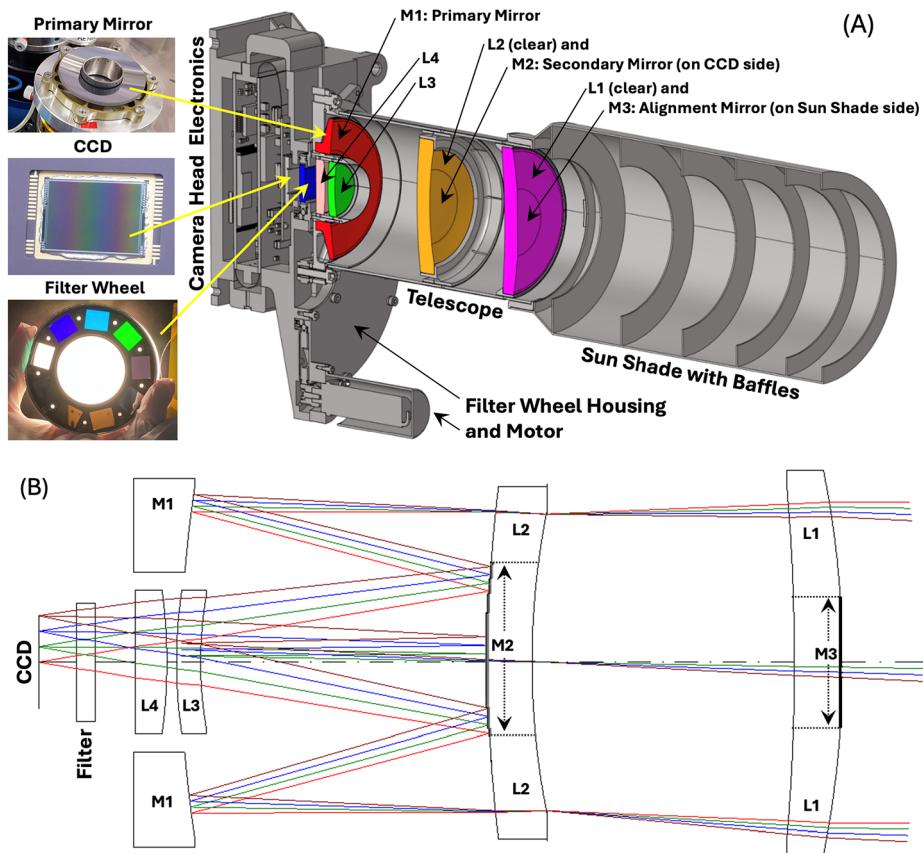
Fig. 4 (A) Cutaway CAD view of the Psyche Multispectral Imager, along with actual photos of some of the key hardware components, including the 57 mm diameter Primary Mirror M1 on a test bench, the ∼12 × 9 mm CCD sensor, and the 9.1 cm diameter filter wheel. (B) Ray trace of the Psyche Multispectral Imager catadioptric telescope, with lens and mirror elements as identified in (A) above. M1 is the spherical primary mirror, and M2 is the spherical secondary mirror, coated onto the back (CCD side) of lens element L2. The part of the front of L2 corresponding to M2 is coated with Z306 diffuse black paint. M3 is a flat-surface mirror coated onto the front of lens element L1 and used for laser alignment verification of camera boresight pointing during pre-flight testing

All of the Imager lens elements and the primary mirror are made of fused silica. Z306 is used for the black coatings on the back sides of mirrors M2 and M3, and the mirrors themselves are silver coated. The lens cells and the optical bench holding the primary are made of Invar 36, and the metering structure and Sun shade are made of graphite cyanate ester (GR/CE) composite. The optics are attached to the filter wheel housing using titanium flexures, and the electronics housing sections are aluminum (7075 alloy).

Over the course of the optics development, the configuration of the optical bench evolved. Initially, it was highly light-weighted, but this proved detrimental to the performance stability of the system over temperature. This configuration thus appears only in non-flight prototypes and a flight spare. A second, more massive revision of the optical bench was found to be much more athermal and was used for the second flight Imager (Imager B). A third revision, which incorporated additional flexures in the primary mirror mounting interface

and which was also measured to be athermal over the required operating temperature range, was used for the primary Imager (Imager A). Analysis, pre-flight testing, and in-flight observations demonstrate that the performance is the same within the uncertainties between the two flight optical benches and meets requirements (Winhold et al. 2025).

Though it is a relatively small effect compared to other parts of the optical system, a slight change of focus was expected between operation under terrestrial ambient conditions and in-flight vacuum conditions, caused by small dimensional changes in the composite metering structure from absorption of water. The magnitude of this effect was modeled and factored into the thickness of the focus spacer used to focus the telescope, and then verified in pre-flight thermal vacuum testing. An external bakeout heater was used to dehydrate the structure by baking it out for $\sim$2 weeks at $+55\,°C$ to $+65\,°C$ shortly after launch.

3.6 Imager Integration and Accommodation

For full block redundancy, there are two independent Imager Camera Heads, one designated "primary" (Imager A) and the second designated as the "backup" (Imager B). Both Camera Heads are mounted next to each other on a common plate within the thermally controlled spacecraft interior volume, with just $\sim$3 cm of each camera's composite Sun shade protruding through holes in the spacecraft's $-X$ panel. The ends of the Sun shades are protected by a "doghouse" enclosure wrapped with multi-layer thermal blanketing (Fig. 5). The DEA is also mounted inside the spacecraft body, but on the inside of the spacecraft's $+Y$ panel. A 2.57 m long roundwire harness connects each independent DEA electronics card to its respective Camera Head.

Both Imager Camera Heads are mounted with the long axis of their CCDs perpendicular to the intended direction of flight over the surface of Psyche. Imager A is boresighted to what will nominally be nadir pointing (parallel to the spacecraft's $-X$ axis), and Imager B is "toed-out" by 3.7° in the $-Y$ direction. Nominally, only Imager A will be operated during the orbital phase of the mission, although both Imagers can be operated simultaneously if desired. The Imager B offset field of view overlaps with Imager A's by $\sim$10%, enabling greater total surface area coverage per unit time if both Imagers are operated simultaneously during some mission phases. Imager B's boresight is also close enough to nadir to serve as the effectively nadir-viewing primary camera, if needed.

4 Psyche Multispectral Imager Testing and Calibration

4.1 Expected Instrument Performance

During the Imager's design phase, we developed a model of the expected radiance incident on the Imager CCD focal plane from sunlight reflected from Psyche based on the average whole-disk telescopic spectrum of the asteroid (summarized in Table 2 of Dibb et al. 2023), and vendor-supplied data on the expected in-flight performance of the CCD, electronics, optics, and filters. We assumed conservative imaging assumptions: heliocentric distance of 3.3 AU, average surface albedo of 0.12, a 70° solar incidence angle, and a relative ground track speed of 120 m/sec (the latter to constrain exposure times to yield $\leq$0.5 pixels of ground motion "smear"; Polanskey et al. 2025). Further, because the CCD and telescope are housed within the thermally controlled spacecraft body to a required temperature range of $-10\,°C$ to $+25\,°C$ and thermally isolated from the Sun Shade, we assumed worst-case expected CCD dark current levels at $+25\,°C$, based on previous in-flight performance of
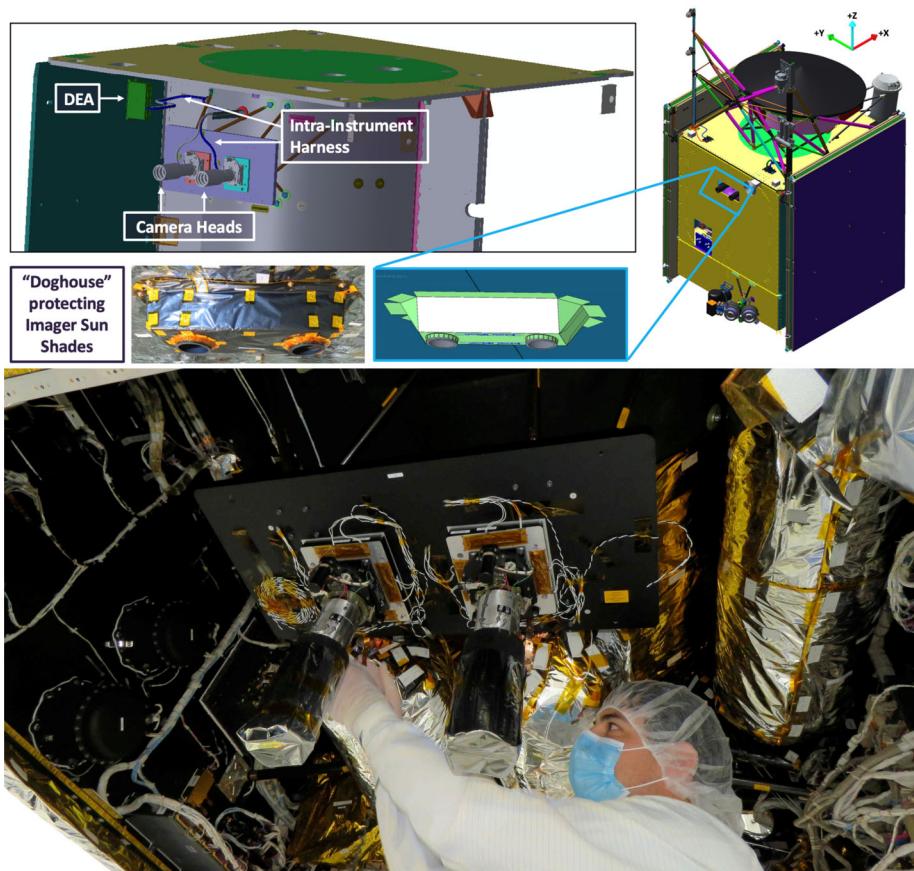
Fig. 5 (Top Right) CAD view of the locations of the Psyche Multispectral Imager Camera Heads, protruding out the $-$X panel of the Psyche spacecraft. The ends of the Imager Sun Shades are protected by a Mylar-blanketed "doghouse" assembly, shown in the CAD view inset and the actual flight configuration to the inset's left. (Top Left) Cutaway CAD view of the inside of the Psyche spacecraft showing the Imager Camera Heads mounted to a rectangular camera plate that is attached by struts to the spacecraft's central structural cylinder. The Imager Digital Electronics Assembly (DEA) is a separate box mounted to the spacecraft's $+$Y panel. The DEA and Camera Heads are connected by a harness. (Bottom) JPL Engineer Stephen Partida finalizing the installation of Imager-A (right) and Imager-B (left) on the Psyche spacecraft [photo credit: Sean Howard, JPL]

this specific CCD sensor (e.g., Bell et al. 2017; Hayes et al. 2020). Under such conservative conditions, our model predicted that the Imager design would yield per-pixel SNR $\geq$ 50 for imaging in all filters, but that 2×2 and 3×3 pixel coadding, respectively, would be required to yield SNR $\geq$ 50 for imaging in the two longest wavelength near-IR filters (near 942 and 1014 nm).

4.2 Instrument Performance Verification and Validation: Pre-Flight Through Cruise

To verify that the as-built Imagers meet the SNR, optical performance, and other imaging requirements predicted during design, and to validate their expected performance at Psyche, each Imager underwent extensive independent testing and calibration in ambient
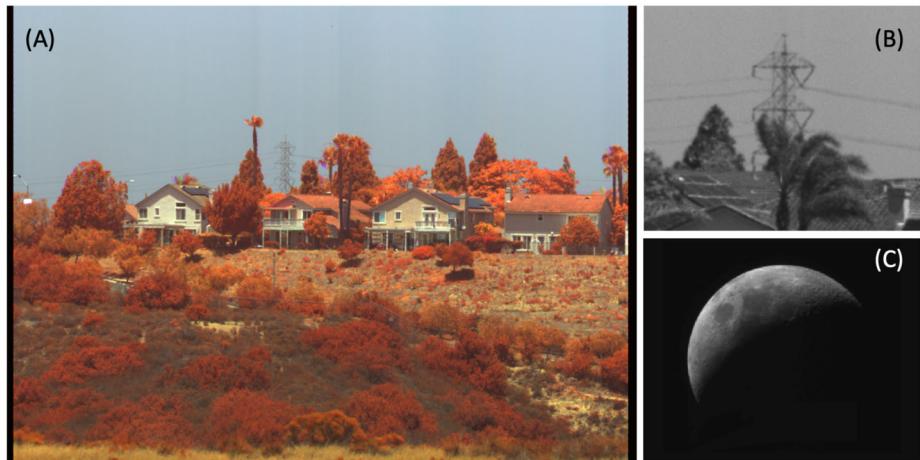
Fig. 6 Examples of "real world" imaging with Imager A in pre-flight testing at MSSS in San Diego. (A) Full frame (1648 × 1200 pixels, including masked reference columns) color composite image of the view out a special cleanroom window of houses on a ridge ∼1 km away. RGB = 722, 548, and 439 nm. (B) Enlarged 548 nm view of power lines ∼2 km away and behind the houses, demonstrating good focus under typical terrestrial imaging conditions. (C) Subset of an Imager A night-time image of the Moon, acquired during relatively clear and dry conditions on Jan. 27, 2022 at 02:26 UTC. The Imager's 50 μrad IFOV (∼10 arcsec on the sky) corresponded to a scale of ∼19 km/pixel on the Moon. Imager B performed similarly under terrestrial conditions

laboratory bench and thermal vacuum chamber conditions at MSSS in San Diego, California, between February 2022 through March 2023, prior to their delivery and installation on the Psyche spacecraft (Winhold et al. 2025). This testing included CCD bias, dark current, read noise, linearity, and full-well characterization; mapping of pixel-to-pixel responsivity ("flatfield") variations; geometric IFOV, FOV, and distortion characterization; assessment of stray and scattered light; quantitative assessment of image quality via measurements of the MTF and PSF; and measurement of the system-level transmission profiles (including out-of-band leakage) and absolute system responsivity for each of the Imager filters. Additional assessment of "real world" image quality was also performed by imaging distant buildings and other structures as well as imaging of the Moon and stars (Fig. 6). Analysis of these pre-flight calibration and characterization images by Winhold et al. (2025) demonstrates that the as-built Imagers meet or exceed their design-based SNR expectations and other requirements (Table 3). A summary of the currently best-known characteristics of the Psyche Multispectral Imagers is provided in Table 4.

Both flight Imagers and the flight DEA underwent individual vibration and pyroshock testing to simulate the vibration and shock environment levels expected during the SpaceX Falcon Heavy launch and Psyche spacecraft deployment processes. No observable changes in optical performance were observed as a result of these tests.

Additional functional testing, boresight determination relative to the spacecraft coordinate system, and basic performance characterization (MTF and relative radiometric responsivity) were also conducted for both Imagers at ambient cleanroom temperature and pressure conditions after the Imagers were installed on and electrically integrated to the Psyche spacecraft at the Astrotech facility in Titusville, Florida, in May and June of 2023. No observable changes in optical performance were observed as a result of spacecraft integration and testing.

Table 4 Psyche Multispectral Imager Instrument Characteristics

Optics	Description
Focus	Fixed; Working distances 800 m to ∞
MTF (optics + filters + CCD)	>0.2 at Nyquist (67.6 lp/mm) between $-10\,°C$ and $+25\,°C$
PSF (optics + filters + CCD)	1.8 ± 0.3 and 2.1 ± 0.2 pixels FWHM for Imagers A and B, respectively[a]
Filter bandpasses	Two 9 position filter wheels: see Table 2
FOV (1600×1200 pix)	$4.6° \times 3.4°$
IFOV (pixel scale)	50 μrad ($\sim$35, 15, 9, and 3.5 m/pix from Orbits A, B1/B2, C, & D; Polanskey et al. 2025)
Focal ratio	$f/2.9$
Effective focal length	148 mm (catadioptric)
Entrance pupil aperture	50.8 mm
1st optic (L1) inner/outer diameter, area	30/60 mm, 2148 mm^2
Primary mirror (M1) in./out. diam., area	32.3/56.9 mm, 1716 mm^2
Primary mirror obscuration ratio	0.508
Optics transmission (total system)	0.781
T/# [$(f/\#) \times$ (sys. transmission)$^{-0.5}$]	$= 2.9 \times (0.508 \times 0.781)^{-0.5} = 4.7$
Pixel solid angle	2.5×10^{-9} sr
Throughput ($A_0 \bullet \Omega$)	5.11×10^{-6} mm^2 sr
Optics Distortion	<0.2%

| Detector & Electronics	Description
CCD	ON Semi (Kodak) KAI-2020M interline transfer, operated in single output mode
Color	Monochrome
Array size	1600×1200 unmasked photoactive pixels (1648×1214 total)
Pixel size	7.4 μm (square pixels)
Preferred Dark Pixels	Left side: Columns 9-15; Right side: Columns 1633-1640 (where first column is 0)
Gain; Read Noise; Full Well (Imager A/B)[a]	$16.1 \pm 0.3/16.3 \pm 0.2$ e$^-$/DN; 12.9 ± 0.1 /13.6 ± 0.1 e$^-$; $30,352 \pm 35/28,202 \pm 21$ e$^-$
Quantum Efficiency	>46% at 550 nm
Radiometric Coeff. (Filter 1: Broadband)	$\sim 3.0 \pm 0.1 \times 10^{-8}$ [(W m^{-2} sr^{-1} nm^{-1}) / (DN/sec]] for both cameras[a]
Pixel Readout Rate	2.5, 5 (default), or 10 Mpix/sec
Digitization	12 bits/pixel optimized for 11-bit dynamic range (0-2047 DN); single gain, no offset states
Data Interface	Synchronous LVDS: 8 Mbit/sec
Command Interface	2 Mbit/sec serial link
Memory	128 MB SDRAM and 8 GB flash buffer ($\sim$4000 raw images) for each camera
Power	5.6 W standby and 8.7 W imaging, per camera

Table 4 (*Continued*)

Exposure	Description
Duration	0 to 838.8 sec; commanded in units of 0.1 msec
Auto-exposure	Based on MSL and MER auto-exposure algorithm (Maki et al. 2003)

Onboard Compression	Description
Uncompressed	12-bit raw data optimized for 11 bits of dynamic range (0-2047 DN)
Lossless	∼1.7:1 lossless predictive compression
Lossy	Realtime JPEG; compression quality 1–100
Companding	12-bit to 8-bit square-root (default) or linear encoding via lookup tables
Video Group of Pictures (GOP)	JPEG-compressed GOPs, ≤2 MB file size and ≤16 frames/GOP
Deferred compression	Images can be stored onboard the DEA uncompressed; specified compression can be performed at a later time for transfer to spacecraft and then downlink

Physical Characteristics	Description
Data Volume: full raw image	$1648 \times 1200 \times 11$ bits = 2.7 MBytes/image
Data Volume: 8-bit companded	$1648 \times 1200 \times 8$ bits = 2.0 MBytes/image
Data Volume: 8-bit + lossless comp.	∼1.2 MBytes/image, assuming ∼1.7:1 lossless compression
Dimensions: CCD Sensor	11.84×8.88 mm (14.8 mm diagonal)
DEA Dimensions	$22 \times 12.2 \times 6.3$ cm
Camera Head	$15.5 \times 11.5 \times 34$ cm (each camera)
Camera pointing	Imager A points nadir (along spacecraft $-X$ axis), Imager B toed-out 3.7° along $-Y$ axis
Mass: Camera Head	1.77 kg each
Mass: DEA	1.58 kg

[a]See Winhold et al. (2025) for more details and in-flight updates.

Shortly after launch in October 2023 and following the bakeout out of the Imager composite structures the following month (see Sect. 3.5), the first sets of in-flight images (of star fields) were acquired from both Imagers in December 2023 and January 2024. These images (Fig. 7) included standard stars and star clusters for radiometric and geometric validation, and long-duration images with the solar blocking filter (Filter 0) in place to assess CCD dark current and noise levels. Quantitative analyses of these results, which met expectations based on pre-flight testing, are reported in Winhold et al. (2025).

During the remainder of the Cruise phase of the Psyche mission, the Imagers will perform periodic maintenance and calibration observations of radiometric standard stars, star clusters, and distant multi-pixel-wide solar system objects (e.g., Jupiter) approximately every six months, a process started in mid-2024. In May 2026, the spacecraft will perform a Mars gravity assist flyby at a range of ∼5750 km (Polanskey et al. 2025), enabling the first in-flight imaging of a well-known field-filling extended object at a scale of ∼300 m/pix at closest approach. Mars flyby Imager data will be used to assess radiometric performance, calibration accuracy, and image quality, and to identify any significant changes in flatfield
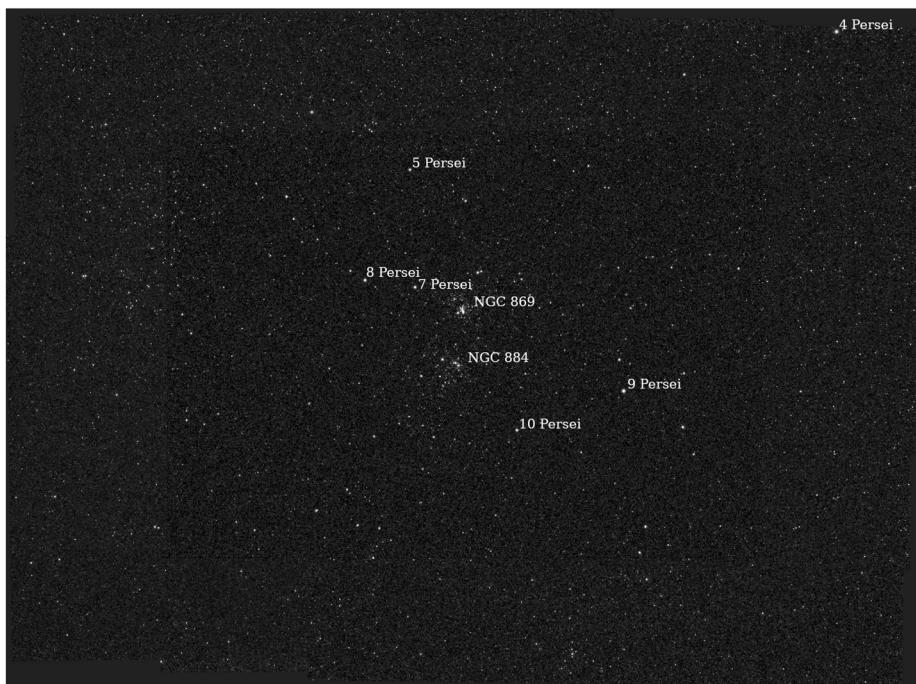
Fig. 7 Example of a 3 × 3 mosaic of images from Imager-B of a star field in the constellation Perseus centered on the famous double cluster NGC869 and NGC884 (also known as h and χ Persei). The images were acquired during initial checkout observations on Jan. 6, 2024. The clusters and some prominent stars are annotated. In-flight focus and performance of both Imagers are comparable based on cruise observations to date

variations (e.g., dust or other particles on the sensors) since pre-flight testing. Additionally, the Mars flyby will serve as a useful practice activity to simulate the later approach to Psyche and to exercise and refine relevant Imager sequencing, data flow, data processing/calibration, and data archiving activities.

5 Prime Mission Operations and Expected Data Products

5.1 Operational Considerations

As described in detail by Polanskey et al. (2025), the Psyche mission's Prime Mission activities are divided into specific phases called Approach, starting shortly after the asteroid begins to be an extended object rather than a point source; Orbits A-D, with nominal altitudes ranging from ∼700 km to ∼75 km; and Transition Orbit periods between Orbits A-D. Here we provide additional details on Imager-related activities and the estimated number and volume of data products (Table 5) planned to be acquired during each of these mission phases.

Table 5 Psyche Multispectral Imager Prime Mission Data Products Summary

Products	Estimated number of files	Estimated data volume (GB)
Raw (Level 0) binary images, all filters	∼85,000	∼350
Calibrated (L1A) Radiance and I/F images, all filters	∼170,000	∼700
Housekeeping data	∼2000	∼3
Pre-launch calibration files	∼1000	<0.5
Calibration Support files	∼120	∼10
Software Interface Specification (SIS) and other processing documents	∼14	negligible
Browse images	∼85,000	∼250
Derived (L1C) global clear image mosaic (20 m/pix scale)	1	∼1
Derived (L1C) global color image mosaics (8 filters, 20 m/pix scale)	8	∼20
Derived (L3) global spectral parameters maps (3-5)	3	∼10
Derived (L3) global topographic map (DTM), from SPG	1	<0.5
Derived (L3) global topographic map (DTM), from SPC	1	<0.5
Derived global geologic map (from orbits B1 + B2)	1	∼3
TOTALS:	**∼ 340,000**	**∼ 1400**

5.1.1 Approach to (16) Psyche

The Psyche mission's Approach phase to Psyche will begin in early 2029, as the asteroid slowly transitions from a small extended object of ∼7 pixels diameter to more than twice the FOV at the end of Approach. During the Approach phase, Imager observations will mostly include OpNav imaging sessions. These sessions consist of imaging the asteroid against fields of background stars, while the asteroid is smaller than the FOV, and a combination of nadir and off-nadir imaging of the asteroid surface during the last week of the Approach phase, when the asteroid greatly exceeds the FOV. The purpose of the OpNav imaging is to assist in the determination of the spacecraft's trajectory relative to the asteroid, to estimate and refine the asteroid's spin state, and to construct the asteroid's shape and topography at increasing resolution, reaching up to 200 m/pix spatial scale at the end of the Approach. Most of the Approach OpNav sessions will span one full asteroid rotational period (∼4.2 hr) and images will be acquired with the clear filter. However multispectral observations through all filters will be included in five OpNav sessions with each camera, to search for early evidence of regional albedo or mineralogic variations and to assist in establishing more accurate exposure estimates for imaging once in orbit. Additional imaging opportunities will include deep time-series surveys to cover the asteroid's Hill sphere of gravitational influence to search for any satellites, rings, or surface activity; and imaging on and off the bright limb of the asteroid, to characterize stray and scattered light within the cameras. Approach imaging will be performed with both Imagers separately to reduce mission risk, although simultaneous observations with both cameras could be used to make collecting the satellite survey imaging mosaic more time efficient, if needed.

5.1.2 Orbit A

The Psyche spacecraft is expected to be captured into a high polar orbit (∼700 km altitude, 90° inclination) around Psyche in mid 2029. Imager observations during this "Orbit

Fig. 8 Images of 433 Eros from the NEAR-Shoemaker mission at the approximate pixel scales representative of those typically expected during the Psyche mission's Orbits A, B1 and B2, C, and D, as labeled
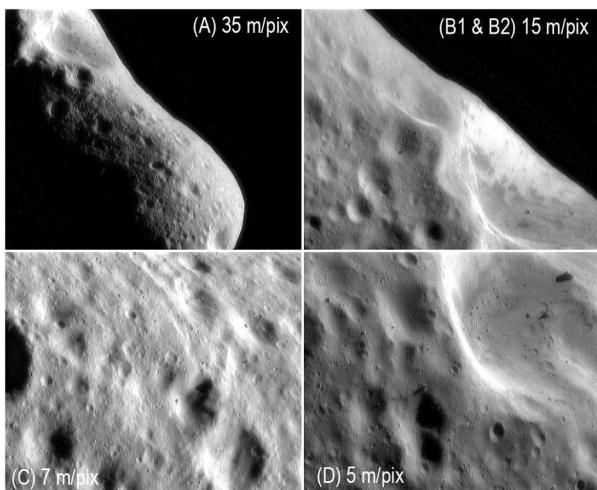
A" phase of the mission, expected to nominally last ∼56 Earth days, will include initial assessment of the asteroid's geology, albedo, and multispectral properties at a relatively low resolution (∼35 m/pixel; e.g., Fig. 8a). The main focus of Orbit A for the Imager investigation will include identifying and characterizing craters and large boulders down to ∼100 m diameter, as well as generating initial global-scale maps of large-scale terrain differences based on albedo, color, morphology, and crater density (Marchi et al. 2022). The majority of Orbit A observations will be conducted at nadir pointing. After the asteroid has been imaged redundantly at nadir, a number of off-nadir observations will be acquired during Orbit A over a total of nine orbital periods. The main purpose of these observations will be to acquire stereo images that enable the estimation of surface topography at close to the image spatial scale, to assist spacecraft navigation for the later science orbits and also to refine the asteroid's spin state that was initially determined during the Approach phase. These observations are planned to be conducted using only Imager A.

5.1.3 Orbit B, Part 1 (Southern Hemisphere)

During an orbit transfer period, the spacecraft will descend to "Orbit B1" (∼300 km altitude, 90° inclination) in late 2029, for approximately three months of global clear filter and multispectral imaging at ∼15 m/pixel scale (e.g., Fig. 8b). Imager observations during this phase of the mission will meet all of the imaging resolution and coverage requirements of the mission (Table 3; see also Polanskey et al. 2025) for the southern hemisphere of Psyche, which is illuminated during this time because of the asteroid's ∼95° obliquity. Meeting these requirements will enable the creation of hemispheric-scale topographic maps for shape modeling, geologic mapping, and topographic mapping (e.g., Jaumann et al. 2022; Zuber et al. 2022), relative age determinations via crater size frequency statistics (e.g., Marchi et al. 2022), as well as assessment of the presence and distribution of both silicates and sulfides on the asteroid's surface (e.g., Dibb et al. 2023).

5.1.4 Orbit D

Then, after a much longer orbit transfer period that includes a transition to a near-equatorial orbit (∼160° inclination), by early 2030 the spacecraft will descend to its lowest Prime Mission altitude of ∼75 km. During this 100-day "Orbit D" phase of the mission, the Imager

will obtain its highest resolution images (up to ∼4 m/pixel; e.g., Fig. 8d), focusing on clear filter imaging for characterization and mapping of smaller (20-30 m diameter) craters, boulders, boulder clusters, and fine surface details regarding potential regolith movement and any features suggestive of volcanic activity or tectonic deformation (e.g., Robinson et al. 2002; Sullivan et al. 2002). A limited amount of multispectral imaging could also be conducted in Orbit D, especially if small-scale features with interesting or anomalous multispectral properties are identified in images from Orbits A or B1. However, the high expected ground track motion in the image plane at this low altitude (∼30 pixels/sec) means that only very short exposure times can be used to keep image smear below 0.5 pixels, limiting the SNR of very high resolution multispectral images. Most imaging will likely be performed using only the primary Imager A camera, although simultaneous observations with both cameras during this low orbit phase could be used to cover more of the surface per unit time with high-resolution images. Imaging in Orbit D is limited to nadir-pointed attitudes and by the volume of data that can be returned to the ground. Margin is built into the nominal Orbit D plan to accommodate any extra time needed transitioning from Orbit B1.

5.1.5 Orbit C

The spacecraft will then ascend to "Orbit C," returning to a near-polar orbital inclination at an altitude of ∼190 km in early 2031. Because of the advancing seasons on Psyche since the beginning of Orbit A, Imager data at ∼10 m/pixel (e.g., Fig. 8c) during this ∼100 day phase of the mission will increase geologic and topographic mapping coverage deeper into the asteroid's northern hemisphere, and will enable the first regional high-resolution multispectral imaging of northern equatorial to mid-latitudes.

5.1.6 Orbit B, Part 2 (Northern Hemisphere)

For the final phase of the Prime Mission, the spacecraft will transition back to an altitude of ∼300 km in mid 2031 for "Orbit B2", to conduct the same kind of imaging study as in Orbit B1, but covering more of the northern hemisphere. Thus, by the end of Orbit B2, Imager observations will have met all of the global imaging resolution and coverage requirements of the mission (Table 3; see also Polanskey et al. 2025).

Approximately two months of additional operations margin are built into the Psyche mission plan, to accommodate potential anomalies or surprises that could cause any of the Orbit phases or the transitions between them to require longer than expected to achieve relevant mission or Imager goals or objectives. The nominal Prime Mission is currently scheduled to end on Nov. 1, 2031. Polanskey et al. (2025) provide significantly more detail about the Psyche mission's nominal expected orbital operations and timeline.

5.2 Imager Commanding, Sequencing, Onboard Image Processing, and Data Management

Commanding of the Imager is performed through ground developed command sequences which are uplinked to the spacecraft and executed at their pre-defined epoch time. For orbital phase imaging, the command sequences make use of reusable sequences, stored onboard the spacecraft's Psyche Compute Element (PCE) computer, that perform repeatable sets of command. At specified times, the PCE sends the commands in those sequences to the Imager DEA, which then commands the Imager Camera Head (CH) electronics to acquire the specified images (potentially sub-framing the image within the CH electronics), change

the required filter, etc. Images are transferred from the CH to the DEA one at a time after acquisition and are stored in the DEA's flash memory as raw Camera Data Products, each with a unique memory location identifier (CDPID). When an image is acquired, the spacecraft Flight Software (FSW) adds the CDPID to a data transfer queue. After the acquisition of a specified number of images (for example, a swath of images across the sunlit dayside of the asteroid during a particular orbital phase), the imaging sequence commands the transfer of the images in the transfer queue, using the desired companding, compression, and/or summing factor, from the Imager DEA to the PCE for eventual downlink to Earth.

DEA processing of Imager data transferred to the PCE is expected to be relatively minimal. Nominally, this is expected to always include companding of the data from 12-bit to 8-bit using a default square-root lookup table developed during pre-flight calibration (Winhold et al. 2025), to avoid downlinking pixel raw signal level variations that correspond to photon shot noise variations, especially at higher DN levels (a strategy used effectively on almost all MSSS deep space cameras on previous NASA missions; e.g., Bell et al. 2017). As an additional processing step, when images are square-root companded (the default behavior), a user-defined bias level (specified by the DC_OFFSET parameter and set to a 12-bit DN level of 110 by default) is automatically subtracted from the 12-bit data before it is companded to 8-bit, to help maximize the dynamic range of the companded images. The DEA can compress images prior to transfer to the PCE using lossless predictive (the default for Imager operations) or lossy JPEG compression. Optionally, the DEA can also be commanded to sum pixels in existing stored images by factors of 2×2, 3×3, or 4×4 pixels (returning the average pixel value) and transmit those smaller images back to the PCE.

The 8 GB of DEA NVM storage can hold ∼4000 raw uncompressed 8-bit images per Imager, so this is a resource that will need to be managed during orbital operations. The NVM used for image storage is allocated using a simple first-fit algorithm without wear leveling. The Imager Operations team at Arizona State University (ASU) will monitor the number of images and their locations in memory for each Imager, using directory and memory dump commands. In general, images will be erased in large groups, with older images being erased before newer ones, and images will only be erased from the DEA after verification of their successful downlink. There must always be enough available memory space (plus margin) to allow for a missed DSN downlink pass without overrunning the DEA NVM.

5.3 Calibration Observations During the Orbital Phases of the Mission

Orbital calibrations will primarily include dark current measurements before or after each swath of imaging of the sunlit surface of the asteroid. Images of standard stars and star clusters for radiometric, pointing, and geometric validation, and imaging on and off the limb of Psyche for stray light characterization, are not planned but could be commanded if required.

5.4 Downlink Assessment and Data Processing/Calibration

Images and other data from the Imagers, DEA, and Imager-relevant spacecraft telemetry channels (e.g., spacecraft-controlled external temperature sensors on/near the Imagers or DEA) are downlinked to Earth through NASA's Deep Space Network and then to the Psyche Mission Operations Center at JPL. The raw images are unpacked from the telemetry stream and converted by JPL into individual 8-bit *.DAT science data and *.EMD telemetry packet files and then into *.IMG files with embedded keyword-value label information that is compliant with NASA Planetary Data System (PDS) 3 Object Description Language (ODL)

format.[1] These images are used by the JPL OpNav team and the Psyche Gravity investigation team (Zuber et al. 2022), and are also immediately converted to Portable Network Graphics (PNG) format images that are posted to the NASA/JPL "Psyche Raw Images" public web site[2] for everyone to enjoy.

The ASU Imager Operations team merges additional relevant telemetry from the temperature sensors external to the Camera Heads and DEA as well as updated image timing and other mission/telemetry information into expanded version of the raw image files that are saved in the Flexible Image Transport System (FITS) file format (e.g., Marmo et al. 2018). The team also generates an associated additional Extensible Markup Language (XML) label file that makes these raw Imager team data products compliant with the NASA PDS4 archive format.[3]

Initial downlink assessment by the Imager Operations team focuses on verifying the health and safety of the Imagers and DEA via monitoring for appropriate temperatures, voltages, and currents in the Imager and spacecraft telemetry. Additional assessments include sequence completion status and run times, data downlink completeness, verification of expected spacecraft pointing, and verification of adequate signal level/SNR in each image. Relevant Imager data and telemetry are captured into an SQL database that is maintained in collaboration with the Psyche mission's Science Data Center (SDC), also located at ASU.

In the event of downlink of incomplete (partial) raw data products or telemetry, Imager operations staff work with the JPL Psyche Mission Operations staff to request retransmits of the missing telemetry packets, and then re-creation of the associated raw images or telemetry data.

Individual raw 8-bit images are calibrated by the Imager operations staff into floating point absolute radiance units (e.g., W/m^2/nm/sr) via the calibration pipeline described by Winhold et al. (2025). The pipeline also creates images further calibrated to radiance factor, also known as "I/F", where I is the observed radiance and πF is the radiance of sunlight incident on the scene at the time of the observation (e.g., Hapke 1993). Like the raw images, individual radiance- and I/F-calibrated images are saved in a NASA PDS4-compliant format, including an external XML label file that contain additional keyword-value information relevant to the calibration of the images.

I/F is comparable to reflectance, enabling comparisons of the Imager's multispectral data to telescopic reflectance spectra of Psyche and other asteroids as well as laboratory reflectance spectra of analogous minerals and meteorites. For isotropically scattering planetary surfaces, I/F divided by the cosine of the solar incidence angle provides an estimate of the surface geometric albedo. More generally, variations of I/F as a function of illumination and viewing geometry can be used to infer information about the physical properties of the surface of Psyche, including particle size, macroscopic surface roughness, and forward vs. backward scattering properties that can inform estimates of surface composition (e.g., Hapke 1993; Gaffey et al. 1993; Clark et al. 2004).

Calibrated clear and multispectral filter images of Psyche will be mosaicked onto a global latitude/longitude grid using the US Geological Survey's Integrated Software for Imagers and Spectrometers (ISIS) routines (e.g., Anderson et al. 2004) and the camera model information needed for orthorectification of images described in Winhold et al. (2025). Clear and color filter image mosaics will be used to create geologic maps, 3-D anaglyphs, and spectral

---

[1]https://pds.nasa.gov/datastandards/pds3/standards.

[2]https://solarsystem.nasa.gov/psyche-raw-images.

[3]https://pds.nasa.gov/datastandards/about.

feature maps used to infer surface composition and/or mineralogy (e.g., Dibb et al. 2023; Polanskey et al. 2025).

Calibrated images acquired over a range of viewing and illumination angles will also be processed via SPC and SPG techniques to create the global shape and topographic models as well as the local/regional DTMs required to achieve a number of primary and Imager-related Psyche mission requirements (Tables 1 and 2; e.g., Jaumann et al. 2022; Zuber et al. 2022). These topographic image products will also be used to generate a number of special 3-D products expected to be useful for education and public outreach, including red/blue anaglyphs, "flyover" movies, and other special products.

5.5 Archive Products

Individual raw and calibrated Imager data products will be archived by the Psyche SDC in the NASA Planetary Data System's Small Bodies Node on approximately 3-month intervals during the orbital mission. Archived images will be compliant with FITS and NASA PDS4 data formats; the former allows the Imager team (and the broader planetary science community) to leverage existing/heritage tools and processes, the latter is a newer data archiving format required by NASA for archiving of all Psyche mission data sets.

Additionally, once the global coverage requirements have been met, a number of additional derived Imager data products will also be archived in the PDS, in PDS4 compliant format. These include global clear-filter and multispectral filter image maps at $\leq$20 m/pixel scale; global spectral parameter maps, including pseudo true color ($\leq$20 m/pixel), sulfide distribution ($\leq$200 m/pixel), and silicate distribution ($\leq$500 m/pixel); a global topographic map derived using SPG methods; a tessellated-plates global shape model derived using SPC methods; and a global geologic unit map (e.g., Jaumann et al. 2022; Zuber et al. 2022; Dibb et al. 2023; Polanskey et al. 2025).

6 Summary

This paper describes the science goals, requirements, design, testing, and initial flight performance of the NASA Psyche mission's Psyche Multispectral Imager ("the Imager") instrument and investigation. The Imager consists of a pair of block redundant 148 mm focal length, $f/2.9$ cameras (and their associated electronics) that are nominally pointed in the nadir direction during orbital imaging of the asteroid (16) Psyche. The primary camera ("Imager A") is pointed along the spacecraft $-X$ axis, and the backup camera ("Imager B") is toed-out by 3.7° to potentially enable greater surface area coverage per unit time if both Imagers are operated simultaneously during some mission phases. Each camera consists of a 1648×1200 active pixel charge-coupled device (CCD) detector and its associated electronics, a 9-position filter wheel assembly that enables broadband polychromatic ($\sim$540 $\pm$ 125 nm) imaging and narrowband color imaging in 7 wavelengths spanning 400-1000 nm, and a multi-baffle Sun shade to minimize scattered light. Each camera has a FOV of 4.6° $\times$ 3.4° and an IFOV of 50 µrad/pixel that enables imaging of the asteroid at scales ranging from $\sim$35 m/pix from 700 km altitude to $\sim$4 m/pix at 75 km altitude. Off-nadir pointing will be used during orbital operations to acquire stereo imaging coverage that enables the creation of surface topographic maps and DTMs with $\leq$50 m vertical precision (e.g., Jaumann et al. 2022). The two Camera Heads are connected to a separate Digital Electronics Assembly (DEA) box that interfaces to the spacecraft avionics and that provides power, commanding, data processing, and onboard image storage. The Imager system shares significant heritage

with imaging instruments flown on the *Mars Climate Orbiter*, *Mars Science Laboratory* and *Mars 2020* rovers, and *Juno*. Additional details about the pre-flight testing and in-flight calibration of the Imagers is provided in a companion paper by Winhold et al. (2025).

Declarations

Competing Interests - Authors M.A. Ravine, M.A. Caplinger, J.A. Schaffner, S.M. Brylow, M.J. Clark, D.A. Peckham, P.T. Otjens, G.J. Price, T. Rowell, and J.W. Ravine are employees of Malin Space Science Systems, Inc., which has a financial interest in the subject matter discussed in this manuscript.

- Author J.D. Laramee is an employee of Motiv Space Systems, Inc., which has a financial interest in the subject matter discussed in this manuscript.

- Authors R.C. Juergens, W. Morgan, and A.G. Parker are employees of II-VI Optical Systems, Inc., which has a financial interest in the subject matter discussed in this manuscript.

- All other authors have no conflicts of interest.

References

Anderson JA, Sides SC, Soltesz DL, Sucharski TL, Becker KJ (2004) Modernization of the integrated software for imagers and spectrometers. In: 35th lunar planet sci conf. Abstract #2039

Bell JF III, Godber A, McNair S, Caplinger MC, Maki JN, Lemmon MT, Van Beek J, Malin MC, Wellington D, Kinch KM, Madsen MB, Hardgrove C, Ravine MA, Jensen E, Harker D, Anderson RB, Herkenhoff KE, Morris RV, Cisneros E, Deen RG (2017) The Mars Science Laboratory Curiosity rover mast camera (mastcam) instruments: pre-flight and in-flight calibration, validation, and data archiving. Earth Space Sci 4:396–452. https://doi.org/10.1002/2016EA000219

Bell JF III, Maki JN, Mehall GL, Ravine MA, Caplinger MA, Bailey ZJ, Brylow S, Schaffner JA, Kinch KM, Madsen MB, Winhold A, Hayes A, Corlies P, Barrington M, Deen R, Cisneros E, Jensen E, Paris K, Crawford K, Rojas C, Mehall L, Joseph J, Proton JB, Cluff N, Betts B, Cloutis E, Coates A, Colaprete A, Edgett KS, Ehlmann BL, Fagents S, Grotzinger J, Tate C, Hardgrove C, Herkenhoff K, Horgan B, Jaumann R, Johnson JR, Lemmon M, Paar G, Caballo-Perucha M, Gupta S, Traxler C, Preusker F, Rice M, Robinson MS, Schmitz N, Sullivan R, Wolff MJ (2020) The Mars 2020 rover mast camera zoom (Mastcam-Z) multispectral, stereoscopic imaging investigation. Space Sci Rev 217:24. https://doi.org/10.1007/s11214-020-00755-x

Bottke WF, Vokrouhlický D, Ballouz RL, Barnouin OS, Connolly HC, Elder C, Marchi S, McCoy TJ, Michel P, Nolan MC, Rizk B, Scheeres DJ, Schwartz SR, Walsh KJ, Lauretta DS (2020) Interpreting the cratering histories of Bennu, Ryugu, and other spacecraft-explored asteroids. Astron J 160:14. https://doi.org/10.3847/1538-3881/ab88d3

Burbine TH, McCoy TJ, Nittler LR, Benedix GK, Cloutis EA, Dickinson TL (2002) Spectra of extremely reduced assemblages: implications for Mercury. Meteorit Planet Sci 37:1233–1244. https://doi.org/10.1111/j.1945-5100.2002.tb00892.x

Bus SJ, Binzel RP (2002) Phase II of the small main-belt asteroid spectroscopic survey: the observations. Icarus 158:106–145. https://doi.org/10.1006/icar.2002.6857

Clark BE, Bus SJ, Rivkin AS, McConnochie T, Sanders J, Shah S, Hiroi T, Shepard M (2004) E-type asteroid spectroscopy and compositional modeling. J Geophys Res 109:1–11. https://doi.org/10.1029/2003JE002200

Cloutis EA (2002) Pyroxene reflectance spectra: minor absorption bands and effects of elemental substitutions. J Geophys Res 107:E6. https://doi.org/10.1029/2001JE001590

Cloutis EA, Gaffey MJ (1991) Pyroxene spectroscopy revisited: spectral-compositional correlations and relationship to geothermometry. J Geophys Res 96:22809–22826. https://doi.org/10.1029/91je02512

Cloutis EA, Hardersen PS, Reddy V, Gaffey MJ, Bailey DT, Craig MA (2009) Metal-orthopyroxene and metal-olivine mixtures: spectral reflectance properties and implications for asteroid spectroscopy. In: 40th lunar planet sci conf. Abstract #1332

Cloutis EA, Hardersen PS, Bish DL, Bailey DT, Gaffey MJ, Craig MA (2010) Reflectance spectra of iron meteorites: implications for spectral identification of their parent bodies. Meteorit Planet Sci 45:304–332. https://doi.org/10.1111/j.1945-5100.2010.01033.x

Dibb SD, Bell JF III, Garvie LA (2021) Reflectance spectra of metal-troilite mixtures: implications for m-/x-type asteroid exploration. In: 52nd lunar planet sci conf. Abstract #1543

Dibb SD, Bell JF III, Garvie L (2022) Spectral reflectance variations of aubrites, metal-rich meteorites, and sulfides: implications for exploration of (16) Psyche and other 'spectrally featureless' asteroids. Meteorit Planet Sci 57:1570–1588. https://doi.org/10.1111/maps.13891

Dibb SD, Bell JF III, Elkins-Tanton LT, Williams DA (Psyche Mission Team) (2023) Visible to near-infrared reflectance spectroscopy of asteroid (16) Psyche: implications for the Psyche mission's science investigations. Earth Space Sci 10:1. https://doi.org/10.1029/2022EA002694

Elkins-Tanton LT, Asphaug E, Bell JF III, Bercovici H, Bills B, Binzel RP, Bottke WF, Dibb S, Lawrence DJ, Marchi S, McCoy TJ, Oran R, Park RS, Peplowski PN, Polanskey CA, Prettyman TH, Russell CT, Schaefer L, Weiss BP, Wieczorek MA, Williams DA, Zuber MT (2020) Observations, meteorites, and models: a pre-flight assessment of the composition and formation of (16) Psyche. J Geophys Res 125:e2019JE006296. https://doi.org/10.1029/2019JE006296

Elkins-Tanton LT, Asphaug E, Bell JF III, Bills B, Bottke W, Jun I, Lawrence D, Marchi S, McCoy T, Merayo J, Oran R, Park R, Peplowski P, Prettyman T, Raymond C, Weiss B, Wieczorek M, Zuber M (2022) Distinguishing the origin of asteroid (16) Psyche. Space Sci Rev 218:17. https://doi.org/10.1007/s11214-022-00880-9

Fornasier S, Migliorini A, Dotto E, Barucci MA (2008) Visible and near infrared spectroscopic investigation of E-type asteroids, including 2867 Steins, a target of the Rosetta mission. Icarus 196:119–134. https://doi.org/10.1016/j.icarus.2008.02.015

Fornasier S, Clark BE, Dotto E, Migliorini A, Ockert-Bell M, Barucci MA (2010) Spectroscopic survey of M-type asteroids. Icarus 210:655–673. https://doi.org/10.1016/j.icarus.2010.07.001

Gaffey SJ, McFadden LA, Nash DB (1993) Ultraviolet, visible, and near-infrared reflectance spectroscopy: laboratory spectra of geologic materials. In: Pieters C, Englert P (eds) Remote geochemical analysis: elemental and mineralogical composition. Cambridge University Press, Cambridge, pp 43–71

Hansen CJ, Caplinger MA, Ingersoll A, Ravine MA, Jensen E, Bolton S, Orton G (2017) Junocam: Juno's outreach camera. Space Sci Rev 213:475–506. https://doi.org/10.1007/s11214-014-0079-x

Hapke B (1993) Theory of reflectance and emittance spectroscopy. Cambridge University Press, New York

Hayes AG, Corlies P, Tate C, Bell JF III, Maki JN, Caplinger M, Kinch KM, Herkenhoff K, Horgan B, Johnson J, Parr G, Rice MS, Jensen E, Kubacki TM, Cloutis E, Ehlmann B, Lakdawalla E, Sullivan R, Winhold A, Barrington M, Parkinson A, van Beek J, Caballo-Perucha P, Cisneros E, Dixon D, Donaldson C, Jensen OB, Kuik J, Lapo K, Magee A (2020) Pre-flight calibration of the Mars 2020 rover mastcam zoom (Mastcam-Z) multispectral, stereoscopic imager. Space Sci Rev 217:29. https://doi.org/10.1007/s11214021-00795-x

Jaumann R, Bell JF III, Polanskey CA, Raymond CA, Aspaugh E, Bercovici D, Bills BR, Binzel R, Bottke W, Christoph JM, Marchi S, Neesemann A, Otto K, Park RS, Preusker F, Roatsch T, Williams DA, Wieczorek MA, Zuber MT (2022) The Psyche topography and geomorphology investigation. Space Sci Rev 218:7. https://doi.org/10.1007/s11214-022-00874-7

Lawrence DJ, Goldsten JO, Peplowski PN, Burks MT, Cheng S, Cully MJ, Effron JM, Elkins-Tanton LT, Espiritu RC, Fix SG, Graziano MB, Hoffer EM, Jun I, Kim G-B, Hines NR, LeBlanc MT, Livingstone EM, Marcotte KM, McCoy TJ, Polanskey CA, Sreekantamurthy M, Yokley ZW (2025) The Psyche Gamma-Ray and Neutron Spectrometer. Space Sci Rev 221

Maki JN, Bell JF III, Herkenhoff KE, Squyres SW, Kiely A, Klimesh M, Schwochert M, Litwin T, Willson R, Johnson A, Maimone M, Baumgartner E, Collins A, Wadsworth M, Elliot ST, Dingizian A, Brown D, Hagerott EC, Scherr L, Deen R, Alexander D, Lorre J (2003) The Mars Exploration Rover Engineering Cameras. J Geophys Res 108:8071. https://doi.org/10.1029/2003JE002077

Malin M, Bell JF III, Calvin W, Clancy RT, Haberle RM, James PB, Lee SW, Thomas PC, Caplinger MA (2001) The Mars color imager (MARCI) on the Mars climate orbiter. J Geophys Res 106:17651–17672. https://doi.org/10.1029/1999JE001145

Malin MC, Calvin WM, Cantor BA, Clancy RT, Haberle RM, James PB, Thomas PC, Wolff MJ, Bell JF III, Lee SW (2008) Climate, weather, and north polar observations from the Mars reconnaissance orbiter Mars color imager. Icarus 194:501

Malin MC, Ravine MA, Caplinger MA, Ghaemi FT, Schaffner JA, Maki JN, Bell JF III, Cameron JF, Dietrich WE, Edgett KS, Edwards LJ, Garvin JB, Hallet B, Herkenhoff KE, Heydari E, Kah LC, Lemmon MT, Minitti ME, Olson TS, Parker TJ, Rowland SK, Schieber J, Sletten R, Sullivan RJ, Sumner DY, Yingst RA, Duston BM, McNair S, Jensen EH (2017) The Mars Science Laboratory (MSL) mast cameras and descent imager: I. Investigation and instrument descriptions. Earth Space Sci 4:506–539. https://doi.org/10.1002/2016EA000252

Marchi S, Asphaug E, Bell JF III, Bottke WF, Jaumann R, Park RS, Polanskey CA, Prettyman TH, Williams DA, Binzel R, Oran R, Weiss B, Russell CT (2022) Determining the relative cratering ages of regions of Psyche's surface. Space Sci Rev 218:24. https://doi.org/10.1007/s11214-022-00891-6

Marchi S, Bell JF III, Bierhaus B, Spencer J (2023) Surface geology of Jupiter's Trojan asteroids. Space Sci Rev 219:44. https://doi.org/10.1007/s11214-023-00985-9

Marmo C, Hare TM, Erard S, Minin M, Pineau FX, Zinzi A, Cecconi B, Rossi AP (2018) FITS format for planetary surfaces: definitions, applications, and best practices. Earth Space Sci 5:640–651. https://doi.org/10.1029/2018EA000388

Mastrodemos N, Rush B, Vaughan A, Owen W (2012) Optical navigation for the Dawn mission at Vesta. In: 23rd International Symposium on Space Flight Dynamics, Pasadena, CA. https://ntrs.nasa.gov/citations/20150004573

Mastrodemos N, Rush PB, Owen WM Jr (2015) Optical navigation for the Rosetta mission. In: AAS guidance and control conference, Breckenridge, Colorado. Paper 15-123

McCoy TJ, Dibb SD, Peplowski PN, Maurel C, Bercovici HL, Corrigan CM, Bell JF III, Weiss BP, Lawrence DJ, Wenkert DD, Prettyman TH, Elkins-Tanton LT (2022) Deciphering redox state for a metal-rich world. Space Sci Rev 218:6. https://doi.org/10.1007/s11214-022-00872-9

ON Semiconductor Inc (2015) KAI-2020 1600 (H) x 1200 (V) Interline CCD Image Sensor. Pub. KAI-2020/D. http://www.onsemi.com/pub/Collateral/KAI-2020-D.PDF

Polanskey CA, Elkins-Tanton LT, Bell JF III, Alonge NK, Bairstow S, Bass D, Biswas A, Cisneros E, Han D, Jun I, Klipstein WM, Lawrence DJ, McCoy T, Mastrodemos N, Merayo J, Noble SK, Oh D, Oran R, Park RS, Peplowski P, Prettyman T, Ream J, Russell CT, Seal D, Weise T, Wenkert D, Weiss BP, Zuber M (2025) Psyche mission description and design rationale. Space Sci Rev 221

Robinson MS, Thomas PC, Veverka J, Murchie SL, Wilcox BB (2002) The geology of 433 Eros. Meteorit Planet Sci 37:1651–1684. https://doi.org/10.1111/j.1945-5100.2002.tb01157.x

Schaffner JA, Caplinger MA, Ravine MA, Hansen CJ, Madsen SN, Berkun AC, Rax BG, Lipkaman Vittling L, Krysak DJ, Johnson MB, Sturm EJ, Delavan JA, Yonter H, Bolton SJ (2025) Recovery of JunoCam by annealing in the Jovian radiation environment. In: IEEE nuclear and space radiation effects conference, Nashville, TN

Sullivan RJ, Thomas PC, Murchie SL, Robinson MS (2002) Asteroid geology from Galileo and NEAR Shoemaker data. In: Bottke WF Jr, Cellino A, Paolicchi P, Binzel RP (eds) Asteroids III. University of Arizona Press, Tucson, pp 331–350

Williams DA, Jaumann R, McSween HY Jr, Raymond CA, Marchi S, Schmedemann N, Russell CT (2014) The chronostratigraphy of protoplanet Vesta. Icarus 244:158–165. https://doi.org/10.1016/j.icarus.2014.06.027

Winhold A, Bell JF III, Caplinger MA, Brylow S, Ravine M, Kubacki T, Dahl-Hansen R, Walworth M, Dibb S, Zhao A, Rodea Y, Cisneros E, Williams D, Warner N, Bates-Tarasewicz H, Monacelli B, Mastrodemos N (2025) Pre-flight and in-flight calibration of the Psyche Multispectral Imagers. Earth Space Sci. to be submitted

Zuber MT, Park RS, Elkins-Tanton LT, Bell JF III, Bruvold KN, Bercovici D, Bills BR, Binzel RP, Jaumann R, Marchi S, Polanskey CA, Raymond CA, Roatsch T, Wang CC, Weiss BP, Wenkert D, Wieczorek MA (2022) The Psyche gravity investigation. Space Sci Rev 218:57. https://doi.org/10.1007/s11214-0

Authors and Affiliations

J.F. Bell III[1] ⓘ · **M.A. Ravine**[2] · **M.A. Caplinger**[2] · **J.A. Schaffner**[2] · **S.M. Brylow**[2] · **M.J. Clark**[2] · **D.A. Peckham**[2] · **P.T. Otjens**[2] · **G.J. Price**[2] · **T. Rowell**[2] · **J.W. Ravine**[2] · **J.D. Laramee**[3] · **R.C. Juergens**[4] · **W. Morgan**[4] · **A.G. Parker**[4] · **D.A. Williams**[1] · **A. Winhold**[1] · **S. Dibb**[1] · **E. Cisneros**[1] · **M. Walworth**[1] · **H. Zigo**[1] · **L. Auchterlonie**[1] · **N. Warner**[5] · **H. Bates-Tarasewicz**[5] · **N. Amiri**[5] · **C. Polanskey**[5] · **N. Mastrodemos**[5] · **R.S. Park**[5] · **N.K. Alonge**[5] · **R. Jaumann**[6] · **R.P. Binzel**[7] · **T.J. McCoy**[8] · **M.G. Martin**[5] · **P.A. Arthur**[5]

✉ J.F. Bell III
     Jim.Bell@asu.edu

[1]   Arizona State University, School of Earth & Space Exploration, Tempe AZ, USA

[2]   Malin Space Science Systems, Inc., San Diego CA, USA

[3]   Motiv Space Systems, Pasadena, CA, USA

[4]   II-VI Optical Systems, Tustin, CA, USA

[5]   Jet Propulsion Laboratory/California Institute of Technology, Pasadena CA, USA

[6]   Freie Universität Berlin, Institute of Geological Sciences, Berlin, Germany

[7]   Massachusetts Institute of Technology, Cambridge, MA, USA

[8]   Smithsonian Institution, Washington, DC, USA